
*Geotechnical and Geological Engineering* **19:** 43–67, 2001.



# Bayesian Estimation of Boundary Conditions with Application to Deep Tunneling

FULVIO TONON, BERNARD AMADEI and ERNIAN PAN
*Department of Civil Engineering, University of Colorado, Boulder, CO 80309-0428, USA.*
*e-mail: tonon@colorado.edu*

(Received 10 July 2000; accepted 16 November 2000)

**Abstract.** An iterative procedure is proposed to determine the far-field state of stress that exists in a rock mass with non-linear behavior around a tunnel. Absolute displacements of the tunnel wall obtained by means of geodetic measurements are used to identify the boundary stress conditions. Previous information is accounted for, so that boundary conditions can be updated at the various stages of a project, as soon as new information becomes available. The application to the 2-D plane strain synthetic model of a tunnel in a yielding rock mass shows the fast convergence of the procedure and the need to use absolute displacements (rather than relative displacements) in order for the identification problem to be well-posed.

**Key words:** identification, Bayesian probability, tunneling monitoring, *in situ* stress, boundary conditions.

## 1. Introduction

The behavior of deep underground excavations in rock is mainly controlled by the state of stress that exists prior to excavation. Determination of the *in situ* state of stress from convergence measurements has attracted the attention of many scholars and practitioners for a long time (e.g. Yang and Sterling, 1989; Sakurai, 1997). In the Under Excavation Technique (UET) (Wiles and Kaiser, 1994a, b) convergence and strain measurements are used to estimate the *in situ* state of stress.

Most studies published in the literature seem to be limited to rock masses that are linearly elastic. When elaso-plastic rock masses are dealt with, *ad hoc* computer programs are used in the literature (e.g. Sakurai et al., 1993; Sakurai and Akutagawa, 1995), so that the procedures proposed are of little use for the practicing engineer. Also, as stressed by Gioda and Maier (1980): 'in practical situations it is generally more convenient to perform, for identification purposes, particular applications of the general computer program to be employed, anyway, for the subsequent analysis, rather than to make recourse to an *ad hoc* formulation of the model.'

In this paper, we introduce a Bayesian iterative algorithm to deal with the non-linear behavior of rock masses (Tonon et al., submitted). Any model (numerical or analytical) of the rock mass and of the excavation can be used, and it is assumed that this model, referred to as model $\mathcal{M}$ in the following, represents the main

mechanisms governing the rock mass behavior (Barla and Gioda, 1983; Purrer, 1997). It is further assumed that a set of displacement, stress, or strain components of the rock mass can be obtained from field measurements. Because a Bayesian approach is adopted, updating information is easily incorporated at successive stages of a project, and subjective judgments based on intuition, experience or indirect information are incorporated systematically with observed data to obtain a balanced estimation.

The iterative procedure is applied to synthetic examples of deep tunnels in yielding rock with and without the presence of a fault. The assumed updating information consists of convergence measurements at the tunnel wall taken behind the tunnel face. The relative importance of the *a priori* and updating information is investigated, as is the importance of their uncertainty. This paper is an extended and revised version of a preliminary, shorter paper (Tonon et al., 2000).

## 2. Identification Procedures

### 2.1. LINEAR MODEL

Consider first a tunnel excavated in a rock mass that can be modeled as linearly elastic in the framework of the small strain and displacement theory (Mardsen and Hughes, 1994). Let us assume that $n$ displacement, strain, or stress components of the rock mass are measured during excavation. Let us also assume that a linear model, $\mathcal{M}$, exists of the tunnel excavation. By virtue of the superposition principle (Mase, 1970), the $k$-th measured component $y_k$ can be related to the $m$ boundary conditions $x_i$ of model $\mathcal{M}$ as:

$$y_k = \sum_{i=1}^{m} h_{ki} \cdot x_i \tag{1}$$

where $h_{\mathrm{ki}}$ is the value of the $k$-th monitored quantity computed by means of $\mathcal{M}$ when $x_i = 1$ and $x_j = 0, j = 1, \ldots, m, j \neq i$.

Due to uncertainty, both measured quantities $y_k$ and boundary conditions $x_{\mathrm{i}}$ are regarded as random variables. In the following, capital italic letters indicate random variables or matrices, and E(.) the mean operator. Let:

- $Y$ be the $n \times 1$ observable random vector, whose $k$-th component is $y_k$.
- $\mathbf{H}$ be the $n \times m$ mapping matrix of rank $m \leqslant n$ (i.e. the problem is assumed to be overdetermined (Menke, 1989)), whose components are $h_{ki}$;
- $X$ be the $m \times 1$ random vector of boundary conditions, whose $i$-th component is $x_{\mathrm{i}}$. An a priori mean and covariance matrix are assumed to be available:

$$\mu_X := \mathbf{E}[X] \tag{2}$$

$$\mathbf{V}_{XX} := \mathbf{E}\left[(X - \mu_X)(X - \mu_X)^T\right] \tag{3}$$

- $U$ be the $n \times 1$ random vector of measurement error such that:

$$\mathbf{E}[U] = \mathbf{0}, \quad \mathbf{E}\left[UU^T\right] = \mathbf{V}, \quad \mathbf{E}\left[UX^T\right] = \mathbf{0} \tag{4}$$

The identification model is thus:

$$Y = \mathbf{H}X + U \tag{5}$$

According to the Gauss–Markov theorem (Lewis and Odell, 1971), the best linear estimator of $X$ is:

$$X = \mu_X - \mathbf{V}_{XX}\mathbf{H}^T\left(\mathbf{H}\mathbf{V}_{XX}\mathbf{H}^T + \mathbf{V}\right)^{-1}\mathbf{H}\mu_X \tag{6}$$

and its covariance matrix is:

$$\mathbf{V}_{\hat{X}} = \mathbf{V}_{XX}\mathbf{H}^T\left(\mathbf{H}\mathbf{V}_{XX}\mathbf{H}^T + \mathbf{V}\right)^{-1}\mathbf{H}\mathbf{V}_{XX} \tag{7}$$

where a superscript 'T' indicates transpose.

### 2.2. NONLINEAR MODEL

Consider now the case in which, due to material non-linearities of model $\mathcal{M}$, the $k$-th measured quantity is a non-linear function, $z_k$, of the boundary conditions:

$$z_k = z_k(x_1, x_2, \ldots, x_m) \tag{8}$$

To illustrate, let us consider two boundary conditions, the extension to more than two variables being straightforward. The theoretical basis of the following iterative procedure is presented by Tonon et al. (submitted), therefore only the outline of the procedure is given here:

(i) At the $j$-th step, by calculating $z_k(x_1^{j-1}, 0)$, the secant value:

$$h_{k1}^j = z_k\left(x_1^{j-1}, 0\right)/x_1^{j-1} \tag{9}$$

is obtained. Similarly, by calculating $z_k(0, x_2^{j-1})$, the secant value $h_{k2}^j = z_k(0, x_2^{j-1})/x_2^{j-1}$ is obtained.

(ii) Calculate:

$$\zeta_k^j = h_{k1}^j \cdot x_1^{j-1} + h_{k2}^j \cdot x_2^{j-1} \tag{10}$$

If $j = 1$, Calculate:

$$\xi_k^1 = z_k\left(x_1^0, x_2^0\right)$$

$$R^0 = \sqrt{\sum_k^n \left(\xi_k^1 - y_k\right)^2 / \sum_k^n (y_k)^2}$$

(iii) If both of the following conditions (a) and (b):

(a) the boundary conditions $\hat{X}^{j-1} = (x_1^{j-1}, x_2^{j-1})$ are such that the relative error $R^{j-1}$ in Eq. (13) is greater than 100%.
(b) the measured stresses, displacements or strains are smaller than the calculated ones, i.e.

$$\xi_k^j - y_k > 0, \quad k = 1, \ldots, n$$

occur, then use the 'simple secant method':

$$y_k^j = y_k \tag{11a}$$

else, use the 'augmented secant method':

$$y_k^j = y_k - \left(\xi_k^j - \zeta_k^j\right) \tag{11b}$$

(iv) The Gauss–Markov theorem, mentioned in Section 2.1, with the observables $y_k^j$ and matrix components $h_{ki}^j$ can be used to calculate a new estimate of the boundary conditions $\hat{X}^j = (x_1^j, x_2^j)$ by means of Eq. (6).
(v) Calculate:

$$\xi_k^{j+1} = z_k\left(x_1^j, x_2^j\right) \tag{12}$$

(vi) Go to point (i) unless the relative error:

$$R^j = \sqrt{\sum_k^n \left(\xi_k^{j+1} - y_k\right)^2 / \sum_k^n (y_k)^2} \tag{13}$$

is less than a specified value or a maximum number of iterations has been achieved.

The reader is referred to Tonon et al. (submitted) for a comparison with the Under Excavation Technique and with other identification procedures proposed in the literature.

The limitations of the procedure proposed are as follows (Tonon et al., submitted):

(a) The procedure fails when $x_i^j = 0$ because, in this case, the ratio in Eq. (9) is meaningless. However, in practice, this limitation can be overcome by using a small value for $x_i^j$ in Eq. (9).
(b) The procedure fails at step (i), if no solution exists for the boundary conditions $y = (0, \ldots, x_i^j, \ldots, 0)$, i.e. if the function $z_k(0, \ldots, x_i^j, \ldots, 0)$ is undefined. Consider, for example, a triaxial test, in which the unknown boundary conditions are the confining (cell) pressure, $X_1$, and the deviator stress, $X_2$. If the soil is cohesionless, the specimen fails under the boundary conditions $x_1 = 0, x_2 > 0$.

## 3. Estimation of *In Situ* State of Stress in Deep Tunneling

A tunnel monitoring program generally involves the measurement of tunnel wall displacements behind the tunnel face. Nowadays absolute displacements can be measured with ease, and without hindering construction (Schubert and Steindorfer, 1996, Rabensteiner, 1996). We assume that the input data (observables) are the tunnel wall absolute displacements measured behind the tunnel face until plane strain conditions are reached. We also assume that a non-linear model $\mathcal{M}$ for the host rock mass exists. The boundary conditions to be estimated are the boundary stresses to be applied to the model.

As a synthetic example, we consider a deep horseshoe-shaped tunnel excavated in phyllite (4.5 m wide, 5 m high), as shown in Figure 1. The rock mass is assumed to be elastic-perfectly plastic. Its strength is described by a Hoek–Brown failure criterion (Hoek and Brown, 1980), and its relevant properties are given in Table 1. The same example is considered by Curran and Corkun (1998). The major and minor *in situ* principal stresses act on the plane orthogonal to the tunnel axis and are equal to 12 MPa and 8 MPa, respectively. The intermediate principal stress is aligned with the tunnel axis and is equal to 10 MPa. The non-linear Finite Element program Phase 2 (Curran and Corkun, 1998) was used for the following calculations.

We assume that we start measuring the tunnel wall displacements behind the tunnel face, when, due to the dome effect (associated with the proximity of the tunnel face), 60% of the total boundary stresses are already applied to the rock mass. The absolute displacements at points A, B, C, D in Figure 1 are assumed to be measured by means of modern geodetic techniques (Rabensteiner, 1996; Schubert and Steindorfer, 1996); only in-plane displacement components are used. These displacements are due to the remaining 40% of the total boundary stresses. Because

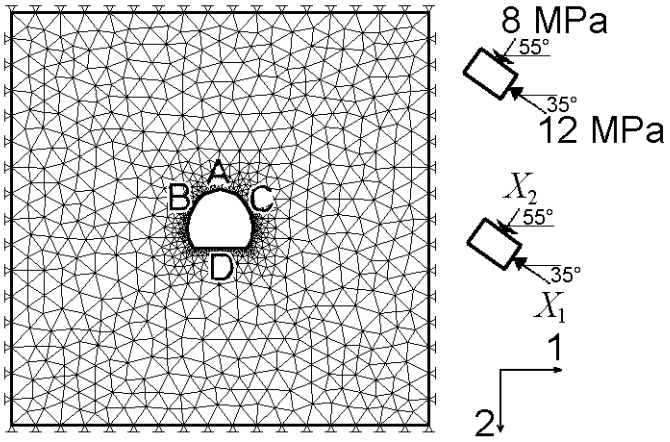


*Figure 1.* Mesh, measurement points and *in situ* state of stress for Examples 1–3. 3-node triangular elements were used for the Finite Element mesh.

Table 1. *Rock mass properties for Examples 1–4.*

| | |
|---|---|
| Young's modulus (MPa) | 1120 |
| Poisson's ratio | 0.3 |
| Failure criterion | Hoek–Brown |
| Uniaxial compr. strength (MPa) | 50 |
| $m$ (peak) | 0.43 |
| $s$ (peak) | 0.00006 |
| Dilation (deg) | 0 |
| $m$ (residual) | 0.43 |
| $s$ (residual) | 0.00006 |

Table 2. *Examples 1–3. Observed absolute tunnel wall displacements (in meters), as projected on (1,2)-axes of Figure 1.*

| Component of vector Y | Description | Value ($m$) |
|---|---|---|
| $y_1$ | horizontal component at A | 0.004 |
| $y_2$ | horizontal component at B | 0.040 |
| $y_3$ | horizontal component at C | –0.050 |
| $y_4$ | horizontal component at D | –0.002 |
| $y_5$ | vertical component at A | 0.050 |
| $y_6$ | vertical component at B | 0.013 |
| $y_7$ | vertical component at C | 0.013 |
| $y_8$ | vertical component at D | –0.060 |

Table 3. *A priori information for Examples 1–4.*

| Example | $\mu_X$ (MPa) | $V_{XX}$ (MPa$^2$) |
|---|---|---|
| 1 | $(4, 2)^T$ | $\begin{pmatrix} 0.8 & 0 \\ 0 & 0.4 \end{pmatrix}$ |
| 2, 4 | $(1, 20)^T$ | $\begin{pmatrix} 0.2 & 0 \\ 0 & 4 \end{pmatrix}$ |
| 3a, 3b | $(20, 30)^T$ | $\begin{pmatrix} 4 & 0 \\ 0 & 6 \end{pmatrix}$ |

the precision obtainable in the field for these measurements is within ±1 mm, the calculated values (in meters) are truncated and rounded at the third digit.

For simplicity, the direction of the principal stresses is assumed to be known (see Figure 1), as is the out-of-plane principal stress (equal to 10 MPa). The first boundary condition ($X_1$) is the principal stress inclined 35° below horizontal, the second boundary condition ($X_2$) is the conjugate principal stress inclined 55° above horizontal.

Four examples, termed Examples 1–4, are considered in the following. In Examples 1–3, the rock mass is homogeneous; the mesh used for the calculations is shown in Figure 1. The observed values of the tunnel wall displacements are given in Table 2. Examples 1–3 differ only in the a priori information, as detailed by Table 3 and portrayed in Figure 2.

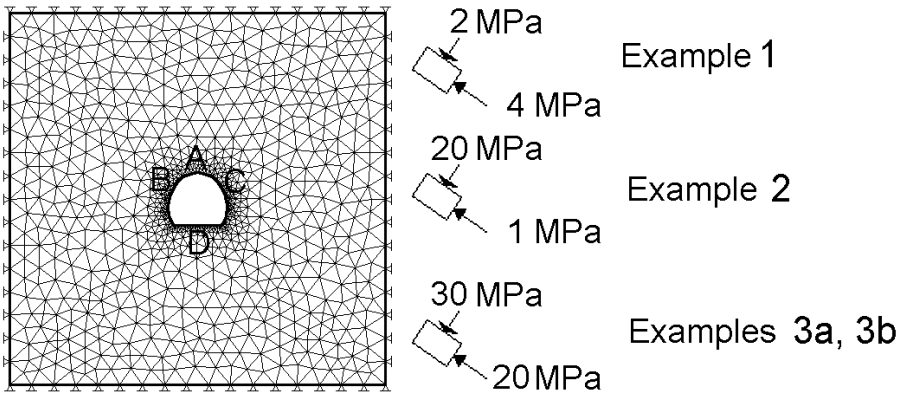


*Figure 2.* Mean *a priori* principal stresses for Examples 1–3.

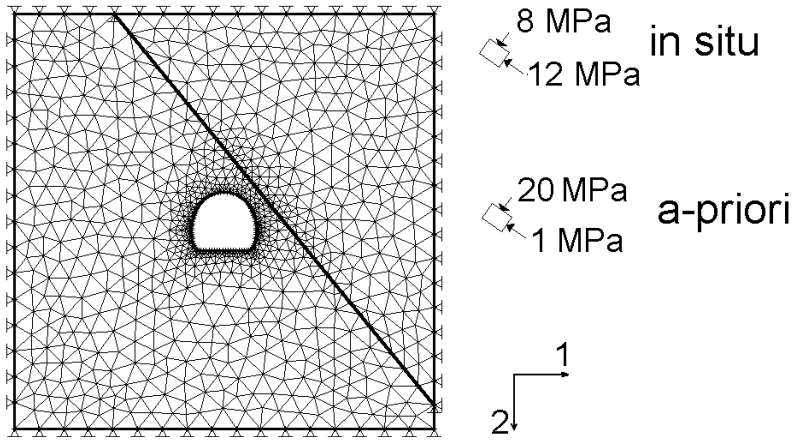


*Figure 3.* FE mesh and mean *a priori* principal stresses for Example 4.

In Example 4, a discontinuity is introduced. It strikes parallel to the tunnel axis, as shown in Figure 3, where the *a priori* mean principal stresses are also portrayed. The *a priori* information and the observed values are given in Tables 3 and 4, respectively.

### 3.1. EXAMPLE 1

The *a priori* information is that the mean value of $X_1$ is equal to 4 MPa and the mean value of the minor principal stress is 2 MPa (see Figure 2 and Table 3).

As for the measurement error, it is assumed to be proportional to the measurement vector $\mathbf{Y}$, given in Table 2, by means of a scalar $S$, i.e. $\mathbf{V} = S\mathbf{Y}$. The smaller $S$ is, the more reliable the measurements are (compared to the *a priori* information). The significance of $S$ will be explored in the following. As for the current calculations,

Table 4. *Example 4. Observed absolute tunnel wall displacements (in meters), as projected on (1,2)-axes of Figure 3.*

| Component of vector Y | Description | Value (*m*) |
|---|---|---|
| $y_1$ | horizontal component at A | 0.012 |
| $y_2$ | horizontal component at B | 0.051 |
| $y_3$ | horizontal component at C | –0.066 |
| $y_4$ | horizontal component at D | 0.001 |
| $y_5$ | vertical component at A | 0.053 |
| $y_6$ | vertical component at B | 0.021 |
| $y_7$ | vertical component at C | 0.023 |
| $y_8$ | vertical component at D | –0.060 |

we regard the displacement measurements as much more reliable than the *a priori* information and set $S = 2*10^{-7}$.

The *a priori* stresses are used as a starting point in the iterative procedure, i.e. $(x_1^0, x_2^0) = (4, 2)$ MPa. Tables 5(a)–(c) give the details of each iteration. In these tables, columns 4, 5, 6, and 8 are obtained as follows:

$$\text{Column 4} = (\text{Column 2})/x_1^{j-1} \tag{14a}$$

$$\text{Column 5} = (\text{Column 3})/x_2^{j-1} \tag{14b}$$

$$\text{Column 6} = (\text{Column 2}) + (\text{Column 3}) \tag{14c}$$

$$\text{Column 8} = y_k - [(\text{Column 7}) - (\text{Column 6})] \tag{14d}$$

Columns 2, 3, and 7 give the results of the FE model when $(x_1 x_2) = (x_1^{j-1}, 0)$, $(x_1, x_2) = (0, x_2^{j-1})$, and $(x_1, x_2) = (x_1^{j-1}, x_2^{j-1})$, respectively.

Table 6 gives the estimated principal stresses at each iteration, along with the relative error. Because the latter is less than 100% at each iteration, the augmented secant method (Eq. 11(b)) was used at each iteration.

Figures 4(a) and 4(b) portray the results of the iterative procedure. The first iteration yields an estimate of the principal stresses that is already very close to the correct answer: the major principal stress is underestimated, whereas the minor principal stress is overestimated. The second iteration overestimates both principal stresses, but the iterative algorithm is capable of correcting itself and the third iteration slightly underestimates both principal stresses. After the third iteration, the relative error is equal to 1.7% (see Table 6). Seeking a better approximation seems unreasonable, given that the observed displacements are known 'only' to within $\pm 1$ mm. The relative error decreases steadily with the number of iterations as plotted in Figure 4(b).

Figure 5 portrays the extent of the plastic zone around the tunnel when the 'true' boundary stresses are applied (see Figure 1). Only the evolution of the plastic zone and of the displacements during the geodetic measurements are shown. The observed radial strain around the opening reaches values in the range of 2–2.5%. It is evident

Table 5(a). *Example 1. Values relative to the first iteration, absolute displacements.*

| $k$ | $z_k(x_1^0, 0) = z_k(4, 0)$ ($m$) | $z_k(0, x_2^0) = z_k(0, 2)$ ($m$) | $h_{k1}^1$ | $h_{k2}^1$ | $\zeta_k^1$ ($m$) | $\xi_k^1$ ($m$) | $y_k^1$ ($m$) |
|---|---|---|---|---|---|---|---|
| (1) | (2) | (3) | (4) | (5) | (6) | (7) | (8) |
| 1 | 0.008297 | –0.005005 | 0.002074 | –0.002503 | 0.003292 | 0.002296 | 0.004996 |
| 2 | 0.011464 | 0.003487 | 0.002866 | 0.001744 | 0.014951 | 0.010865 | 0.044086 |
| 3 | –0.010413 | –0.006360 | –0.002603 | –0.003180 | –0.016773 | –0.011797 | –0.054976 |
| 4 | –0.008822 | 0.005219 | –0.002205 | 0.002610 | –0.003603 | –0.003043 | –0.002560 |
| 5 | 0.007469 | 0.007621 | 0.001867 | 0.003811 | 0.015090 | 0.010943 | 0.054147 |
| 6 | 0.008350 | –0.004205 | 0.002087 | –0.002103 | 0.004145 | 0.005391 | 0.011754 |
| 7 | –0.005769 | 0.007286 | –0.001442 | 0.003643 | 0.001517 | 0.001538 | 0.012979 |
| 8 | –0.010000 | –0.009107 | –0.002500 | –0.004554 | –0.019107 | –0.012971 | –0.066136 |

Table 5(b). *Example 1. Values relative to the second iteration, absolute displacements.*

| $k$ | $z_k(x_1^1, 0)$ ($m$) | $z_k(0, x_2^1)$ ($m$) | $h_{k1}^2$ | $h_{k2}^3$ | $\zeta_k^2$ ($m$) | $\xi_k^2$ ($m$) | $y_k^2$ ($m$) |
|---|---|---|---|---|---|---|---|
| (1) | (2) | (3) | (4) | (5) | (6) | (7) | (8) |
| 1 | 0.017406 | –0.011868 | 0.001519 | –0.001465 | 0.005538 | 0.003740 | 0.005798 |
| 2 | 0.030955 | 0.015424 | 0.002701 | 0.001903 | 0.046379 | 0.038568 | 0.047811 |
| 3 | –0.033110 | –0.015514 | –0.002889 | –0.001914 | –0.048624 | –0.047198 | –0.051426 |
| 4 | –0.017309 | 0.011865 | –0.001510 | 0.001464 | –0.005444 | –0.000975 | –0.006469 |
| 5 | 0.026518 | 0.019428 | 0.002314 | 0.002397 | 0.045946 | 0.046662 | 0.049284 |
| 6 | 0.021048 | –0.005443 | 0.001836 | –0.000672 | 0.015605 | 0.012568 | 0.016037 |
| 7 | –0.010316 | 0.017916 | –0.000900 | 0.002211 | 0.007600 | 0.012075 | 0.008525 |
| 8 | –0.034659 | –0.022993 | –0.003024 | –0.002837 | –0.057652 | –0.056753 | –0.060899 |

Table 5(c). *Example 1. Values relative to the third iteration, absolute displacements.*

| $k$ | $z_k(x_1^2, 0)$ ($m$) | $z_k(0, x_2^2)$ ($m$) | $h_{k1}^3$ | $h_{k2}^3$ | $\zeta_k^3$ ($m$) | $\xi_k^3$ ($m$) | $y_k^3$ ($m$) |
|---|---|---|---|---|---|---|---|
| (1) | (2) | (3) | (4) | (5) | (6) | (7) | (8) |
| 1 | 0.018318 | –0.012179 | 0.001810 | –0.001423 | 0.006139 | 0.003664 | 0.006475 |
| 2 | 0.032938 | 0.016998 | 0.003254 | 0.001986 | 0.049936 | 0.042491 | 0.047445 |
| 3 | –0.035650 | –0.016550 | –0.003522 | –0.001934 | –0.052200 | –0.052254 | –0.049946 |
| 4 | –0.018089 | 0.012307 | –0.001787 | 0.001438 | –0.005782 | –0.001705 | –0.006077 |
| 5 | 0.029051 | 0.020744 | 0.002870 | 0.002424 | 0.049795 | 0.051496 | 0.048299 |
| 6 | 0.022380 | –0.004919 | 0.002211 | –0.000575 | 0.017461 | 0.013150 | 0.017311 |
| 7 | –0.010692 | 0.018847 | –0.001056 | 0.002202 | 0.008155 | 0.014133 | 0.007022 |
| 8 | –0.037756 | –0.024235 | –0.003730 | –0.002832 | –0.061991 | –0.062426 | –0.059565 |

that the problem is highly non-linear, and that the limits of applicability for the small strain theory are reached. The FE program Phase 2 is based on small strain theory.

Now, the advantages in using absolute displacements, rather than traditional relative displacements (generally measured by means of tape extensometers), are investigated. To do so, let us consider the in-plane relative displacements between

Table 6. *Example 1. Estimated stresses and relative error, absolute displacements.*

| Iteration $j$ | $(x_1^j, x_2^j)$ (MPa) | $R_j = \sqrt{\frac{\sum_k^8 \left(\xi_k^{j+1} - y_k\right)^2}{\sum_k^8 (y_k)^2}}$ (%) |
|---|---|---|
| 1 | (11.4621, 8.1035) | 5.7 |
| 2 | (12.1209, 8.5582) | 3.6 |
| 3 | (11.8202, 7.9730) | 1.7 |

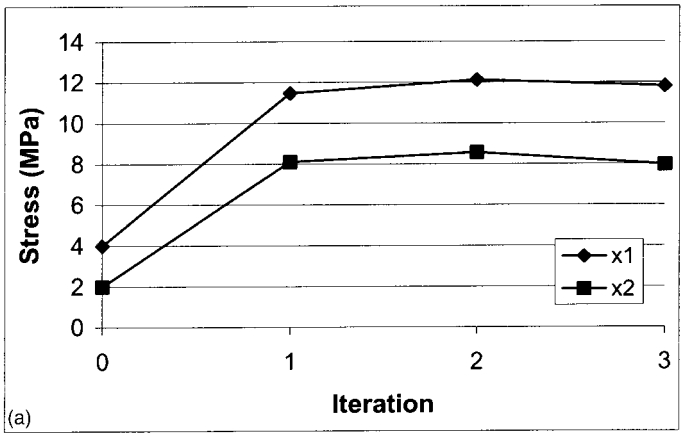


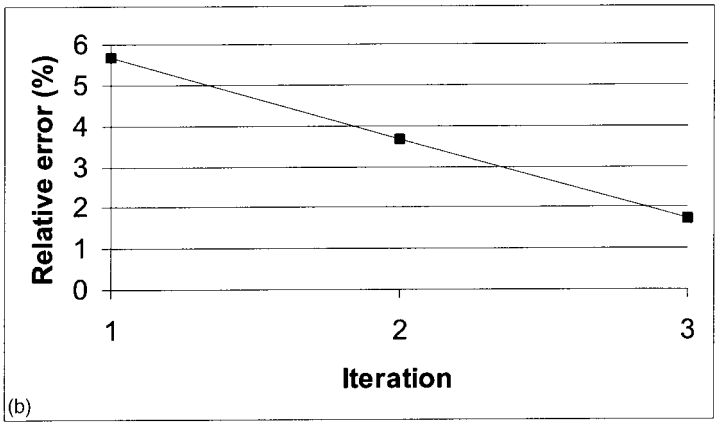


*Figure 4.* (a) Example 1, computed boundary stresses at each iteration (iteration = 0 refers to the starting state of stress); (b). Example 1, square mean root of the difference calculated-measured displacements at each iteration.

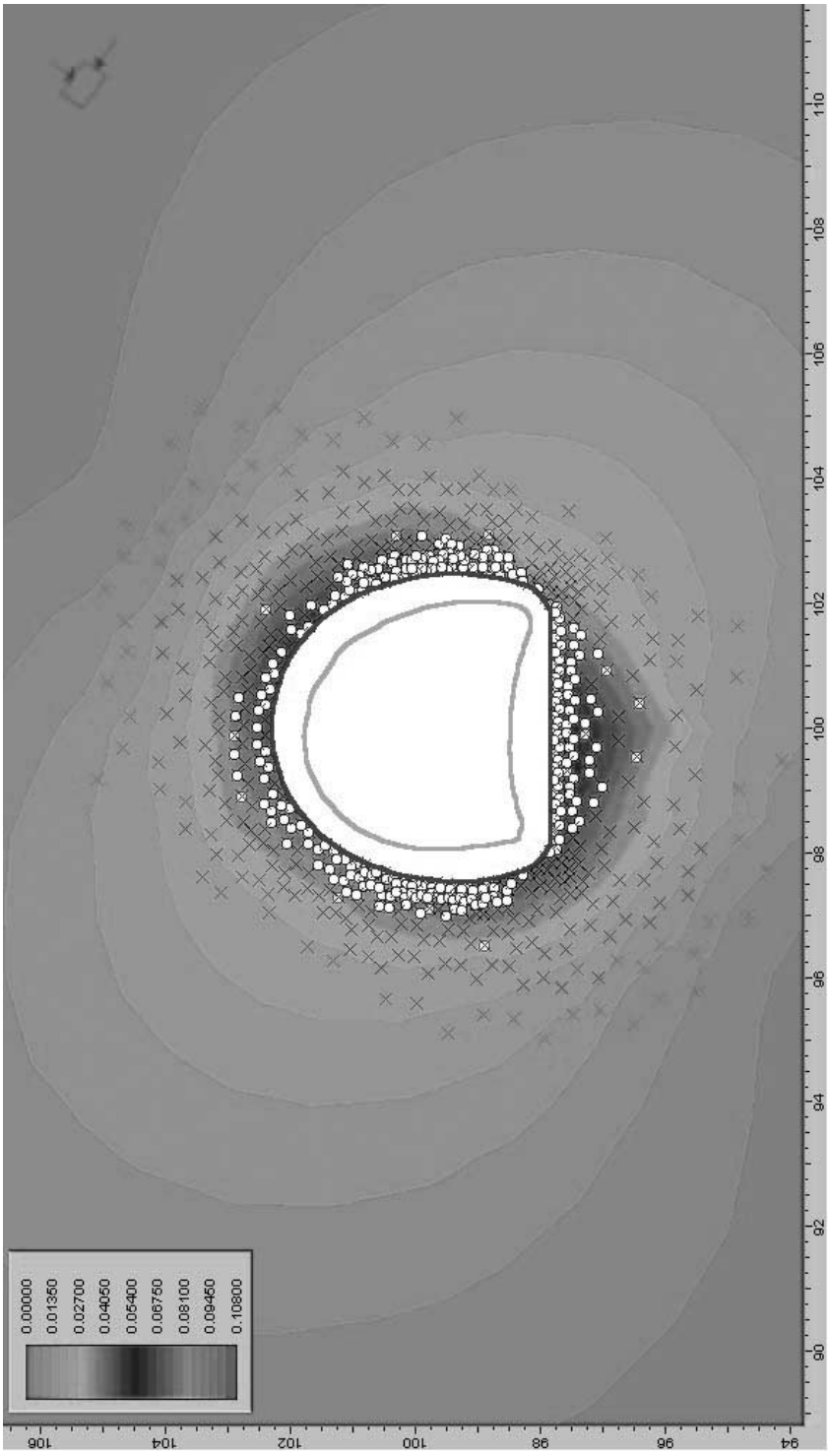


*Figure 5.* Contours of displacement vector magnitude (m). A cross indicates an element yielded in shear, a white dot an element failed in traction. Difference between stage 2 (end of geodetic measurements) and stage 1 (beginning of geodetic measurements).

Table 7(a). *Example 1. Relative measured tunnel wall displacements (m).*

| Component of vector Y | Description ($y_k$ values are given in Table 4.3) | Value (*m*) |
|---|---|---|
| ${}_{rel}y_1$ | Relative displacement A–B $\sqrt{(y_1 - y_2)^2 + (y_5 - y_6)^2}$ | 0.051623 |
| ${}_{rel}y_2$ | Relative displacement A–C $\sqrt{(y_1 - y_3)^2 + (y_5 - y_7)^2}$ | 0.059034 |
| ${}_{rel}y_3$ | Relative displacement B–C $\sqrt{(y_2 - y_3)^2 + (y_6 - y_7)^2}$ | 0.010000 |
| ${}_{rel}y_4$ | Relative displacement A–D $\sqrt{(y_1 - y_4)^2 + (y_5 - y_8)^2}$ | 0.110160 |

Table 7(b). *Example 1. Values relative to the first iteration, relative displacements.*

| $k$ | ${}_{rel}z_k(x_1^0, 0) = {}_{rel}z_k(4, 0)$ (*m*) | ${}_{rel}z_k(0, x_2^0) = {}_{rel}z_k(0, 2)$ (*m*) | ${}_{rel}h_{k1}^1$ | ${}_{rel}h_{k2}^1$ | ${}_{rel}\zeta_k^1$ (*m*) | ${}_{rel}\xi_k^1$ (*m*) | ${}_{rel}y_k^1$ (*m*) |
|---|---|---|---|---|---|---|---|
| (1) | (2) | (3) | (4) | (5) | (6) | (7) | (8) |
| 1 | 0.003287 | 0.014559 | 0.000822 | 0.007280 | 0.017847 | 0.010210 | 0.059259 |
| 2 | 0.022920 | 0.001396 | 0.005730 | 0.000698 | 0.024315 | 0.016943 | 0.066406 |
| 3 | 0.026037 | 0.015133 | 0.006509 | 0.007567 | 0.041171 | 0.022987 | 0.028183 |
| 4 | 0.024459 | 0.019605 | 0.006115 | 0.009803 | 0.044064 | 0.024503 | 0.129721 |

points A, B, C and D in Figure 1, as defined in Table 7(a). Table 7(b) gives the values for the first iteration, when relative displacements are used as observed data. Figures 6(a) and 6(b) illustrate the different results obtained at the first iteration when using absolute displacements or relative displacements, respectively. These figures show that:

(a) When $S$ is large, i.e. comparable with the coefficient of variation of the *a priori* information, the estimated values are equal to the *a priori* values. This occurs when using either absolute or relative displacements.
(b) When $S$ diminishes and absolute displacements are used, the estimated values of the boundary stresses tend monotonically to a plateau, which is very close to the actual state of stress.
(c) When $S$ diminishes and relative displacements are used, the estimated value of $X_1$ initially increases, but eventually decreases and becomes less than the estimated value of $X_2$. This yields not only wrong values for the boundary stresses, but also a wrong picture of the principal stress orientation.

These results clearly highlight the difficulty in using relative displacements when estimating the *in situ* state of stress in a yielding rock mass. In fact, in this case

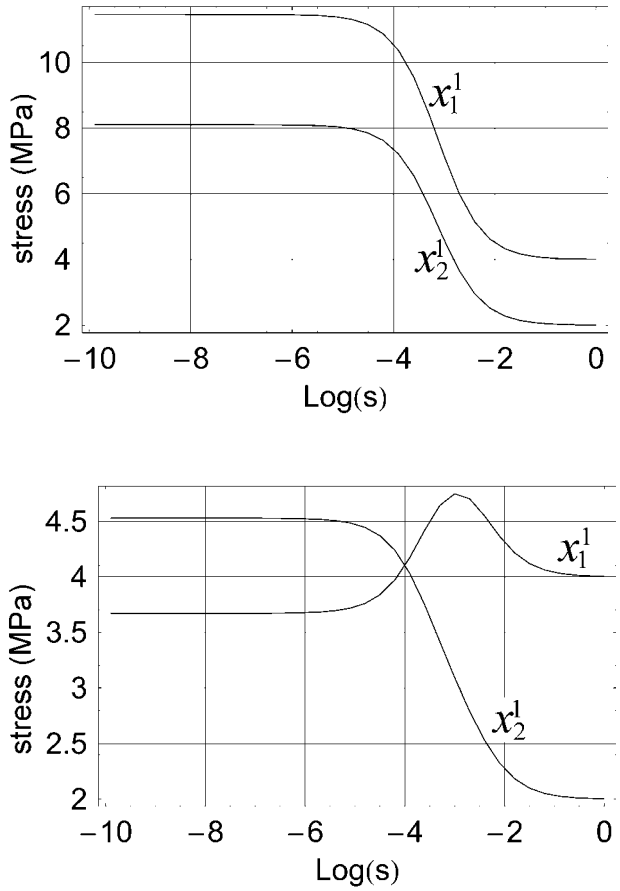


*Figure 6.* Example 1. Best estimates of boundary stresses versus $S$ at the first iteration using: (a) absolute displacements as observed data; (b) relative displacements as observed data.

the problem turns out to be very ill-posed because many different displacement fields around the tunnel may give the same relative displacements at the tunnel walls. Accordingly, many *in situ* states of stress exist that give the same relative displacements at the tunnel walls.

### 3.2. EXAMPLE 2

In this example, the *a priori* information is that the major principal stress of 20 MPa is inclined 55° above horizontal and the minor principal stress is 1 MPa (see Figure 2 and Table 3). Finally, we set $S = 2^{*}10^{-7}$ and $(x_1^0, x_2^0) = (1, 20)$.

The results of the iterative procedure are given in Table 8, and plotted in Figure 7(a)–(b). Because the relative error was less than 100% (see Table 8), the augmented secant method was used at each iteration. When compared to the actual state of

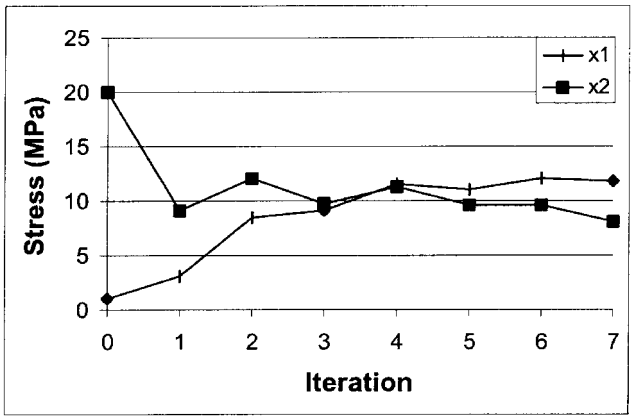


(a)

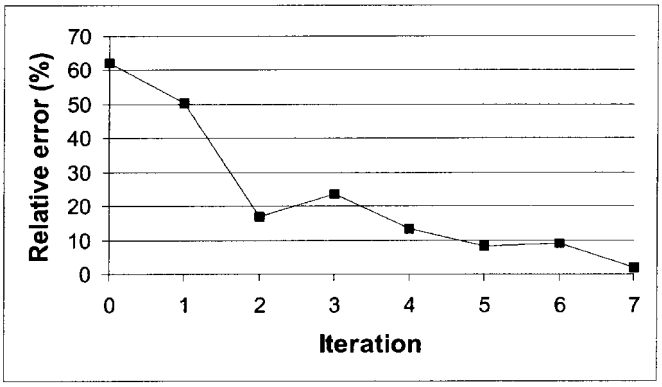


(b)

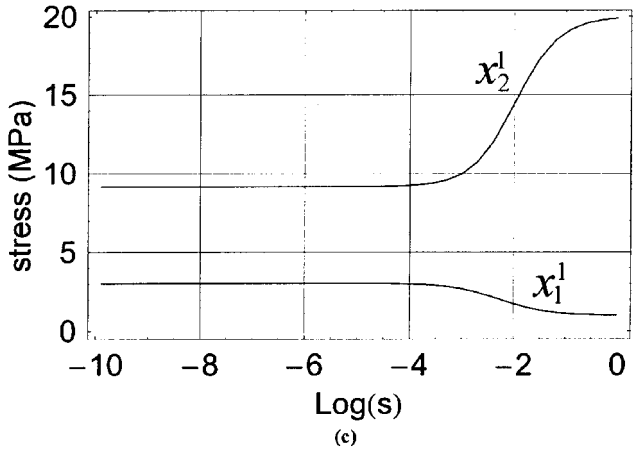


(c)

*Figure 7.* Example 2. (a) Computed boundary stresses at each iteration (iteration = 0 refers to the starting state of stress); (b) square mean root of the difference calculated-measured displacements at each iteration; (c) best estimates of boundary stresses versus $S$ at the first iteration using absolute displacements as observed data.

Table 8. *Example 2. Estimated stresses and relative error.*

| Iteration $j$ | $(x_1^j, x_2^j)$ (MPa) | $R_j = \sqrt{\dfrac{\sum_k^8 \left(\xi_k^{j+1} - y_k\right)^2}{\sum_k^8 (y_k)^2}}$ (%) |
|---|---|---|
| 1 | (3.0270, 9.1600) | 50.18 |
| 2 | (8.4120, 9.7373) | 16.71 |
| 3 | (9.1364, 9.7373) | 23.55 |
| 4 | (11.5639, 11.255) | 13.27 |
| 5 | (11.0679, 9.6443) | 8.42 |
| 6 | (12.0839, 9.5745) | 9.18 |
| 7 | (11.8156, 8.1183) | 1.94 |

stress (Figure 1), the first *a priori* stress appears to be very low, and the second *a priori* stress appears to be very high. Nonetheless, the procedure converges in seven iterations to the correct values of the boundary stresses, despite the fact that the starting boundary conditions were completely wrong and the major and minor in-plane stress directions were interchanged. The relative error is not monotonically decreasing with the number of iterations.

The graphs of the estimated boundary stresses versus $S$ at the first iteration are shown in Figure 7(c). The problem is well posed because both stresses reach monotonically a plateau when $S$ goes to zero, and the major and minor principal stress directions do not change when $S$ goes to zero.

### 3.3. EXAMPLES 3A AND 3B

In these two examples, the *a priori* information is that the major principal stress of 30 MPa is inclined 55° above horizontal and the minor principal stress is 20 MPa (see Figure 2 and Table 3). These stresses are both much larger than the actual ones, and the principal stress directions are interchanged. Finally, we set $S = 2^{*}10^{-7}$ and $(x_1^0, x_2^0) = (20, 30)$.

The relative error $R^0$ is equal to 381% (see Table 9), and all calculated displacements are larger than the measured ones. Tonon (2000) showed that, under these conditions, the augmented secant procedure (Eq. 11(b)) may not converge, and the simple secant procedure (Eq. 11(a)) should be used instead.

In order to exemplify the type of problems that may be encountered, in Example 3a the augmented secant procedure (Eq. 11(b)) was used throughout. The estimated boundary conditions and the calculated relative errors are given in Table 9, and are plotted in Figures 8(a)–(b). It is shown that convergence is not achieved: rather a typical oscillating behavior is displayed. Also, the estimated boundary stresses have non negligible tensile values at iterations 1, 3, and 5 (see Table 9). The stability

Table 9. *Example 3(a). Estimated stresses and relative error.*

| Iteration $j$ | $(x_1^j, x_2^j)$ (MPa) | $R_j = \sqrt{\frac{\sum_k^8 \left(\xi_k^{j+1} - y_k\right)^2}{\sum_k^8 (y_k)^2}}$ (%) |
|---|---|---|
| 0 | (20, 30) | 381.06 |
| 1 | (–12.4624, 3.9269) | 100.60 |
| 2 | (22.4280, 16.9614) | 223.02 |
| 3 | (7.6298, –5.8499) | 83.00 |
| 4 | (26.4047, 20.0328) | 284.11 |
| 5 | (11.0741, –3.7735) | 70.86 |

Table 10. *Example 3(b). Estimated stresses and relative error.*

| Iteration $j$ | $(x_1^j, x_2^j)$ (MPa) | $R_j$ (%) |
|---|---|---|
| 0 | (20, 30) | 381.06 |
| 1 | (7.8678, 7.5432) | 43.20 |
| 2 | (11.1883, 10.5889) | 8.47 |
| 3 | (9.7915, 8.6916) | 23.80 |
| 4 | (12.4219, 10.4914) | 19.40 |
| 5 | (11.5458, 7.9947) | 5.40 |

analysis at the first iteration (Figure 8(c)) indicates that $x_2^1$ is always greater than $x_1^1$, and that $x_2^1(S)$ presents a local minimum.

Convergence can easily be achieved if the correction factor $\xi_k$ is disregarded in the first iterations according to point (iii) of the procedure in Section 2.2. In Example 3(b), the simple secant procedure was adopted until the relative error stabilized below 100%. When the relative error was less than 100%, the augmented secant procedure was resumed. In the present case, the simple secant procedure was used in the first 3 iterations, and the augmented secant procedure for the remaining iterations. The results shown in Table 10, and Figures 9(a)–(b) indicate that the adopted strategy leads to fast convergence, even in this difficult situation. The stability analysis at the first iteration (compare Figure 9(c) with Figure 8(c)) indicates that in this case the solution is more stable because both functions $x_1^1(S)$ and $x_2^1(S)$ do not present local minima.

### 3.4. EXAMPLE 4

Let us consider the same tunnel, rock mass properties (as given in Table 1), and *a priori* estimates of the state of stress as in Example 2 (see Table 3). Compared to Example 2, a fault strikes parallel to the tunnel axis, and dips as shown in Figure 3.

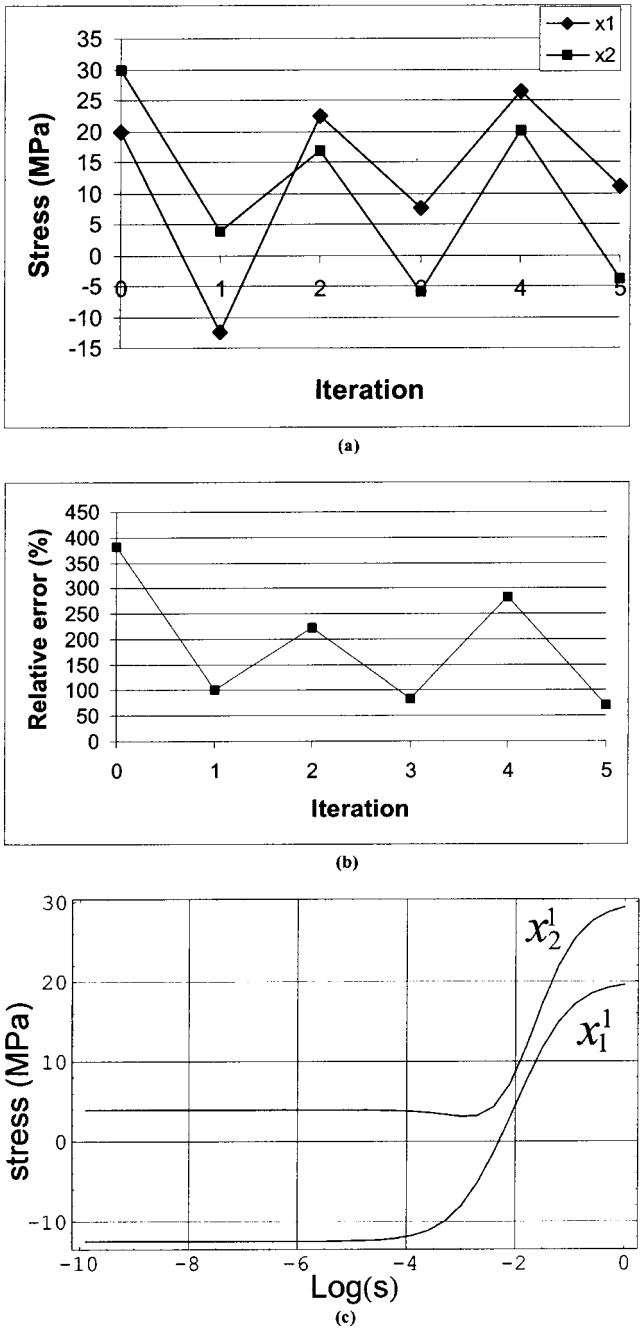


*Figure 8.* Example 3(a). (a) Computed boundary stresses at each iteration (iteration = 0 refers to the starting state of stress); (b) square mean root of the difference calculated-measured displacements at each iteration; (c) best estimates of boundary stresses versus $S$ at the first iteration using absolute displacements as observed data.

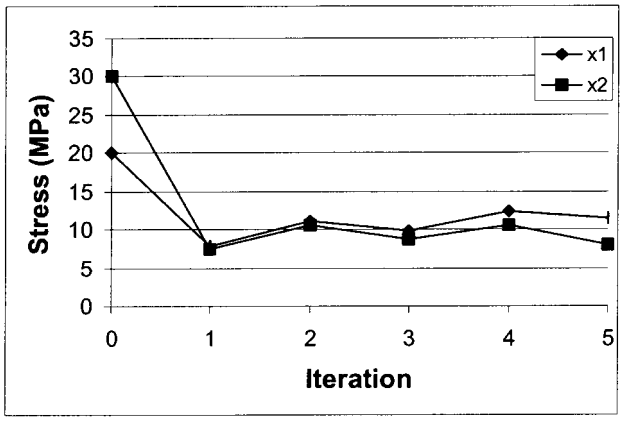


(a)

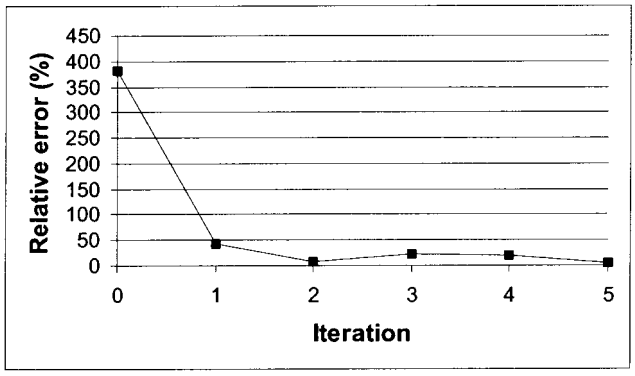


(b)

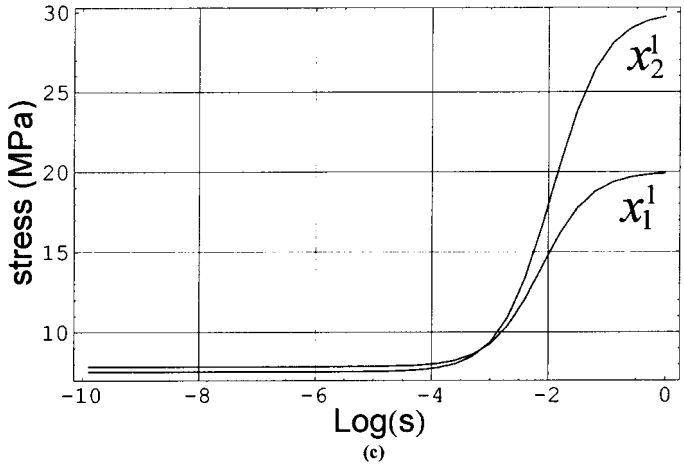


(c)

*Figure 9.* Example 3(b). (a) Computed boundary stresses at each iteration (iteration = 0 refers to the starting state of stress); (b) square mean root of the difference calculated-measured displacements at each iteration; (c) best estimates of boundary stresses versus $S$ at the first iteration using absolute displacements as observed data.

The normal stiffness of the fault is assumed to be equal to 2500 MPa/m, and its shear stiffness is equal to 1000 MPa/m. A Coulomb failure criterion is adopted, with zero tensile strength, a friction angle of 5°, and zero cohesion. Such a low resistance along the fault makes the problem even more non-linear than in Examples 1–3. In fact, Figures 10(a) and (b) show the clear discontinuity in the stress and displacement fields caused by the fault. Figure 10(c) plots the shear relative displacements along the discontinuity induced by tunnel excavation.

As in Examples 1–3, we assume that 60% of the *in situ* state of stress is applied before measurements are taken, and that the remaining 40% causes the change in the displacement field captured by the displacement measurements. The measured absolute displacements at points A to D (Figure 1) are given in Table 4.

The results of the iterative procedure are given in Table 11, and illustrated in Figures 11(a) and 11(b). Because the relative error was always less than 100%, the augmented secant procedure (Eq. 11(b)) was used throughout. One can observe that the solution converges quickly to the exact values as soon as $x_1^j$ becomes larger than $x_2^j$ (this happens at iteration 5). Only six iterations are sufficient in order to arrive at the correct values of the boundary conditions, in spite of the high degree of non-linearity involved in this problem. Figure 11(c) shows that the identification problem is well constrained and stable.

## 4. Conclusions

The applicability to tunneling of a Bayesian iterative procedure for boundary condition estimation has been investigated.

The proposed iterative algorithm shows fast convergence rates and stability even in the presence of significant material non-linearities. Fast convergence rate is of vital importance when using large and complex numerical models, in order to minimize computational time.

Stability depends not only on the iterative algorithm, but also on the basic data. Specifically, it is shown that it is necessary to use absolute displacement measurements as opposed to traditional relative displacement measurements in order for the identification problem to be well-posed. Traditional relative convergence measurements may lead to completely wrong conclusions about the *in situ* state of stress and to unacceptable sensitivity of the estimated *in situ* state of stress on measurement errors.

Although, in this paper, for illustration purposes, displacement components have been used as basic data and rock stresses as boundary conditions, the algorithm is quite general because mixed basic data (displacement components, stresses, strains) and mixed boundary conditions (stresses, displacement components) may be used without difficulty. Also, any model of the rock mass can be used, thus engineers can continue utilizing their own software used for analyzing the rock mass and the tunnel excavation.

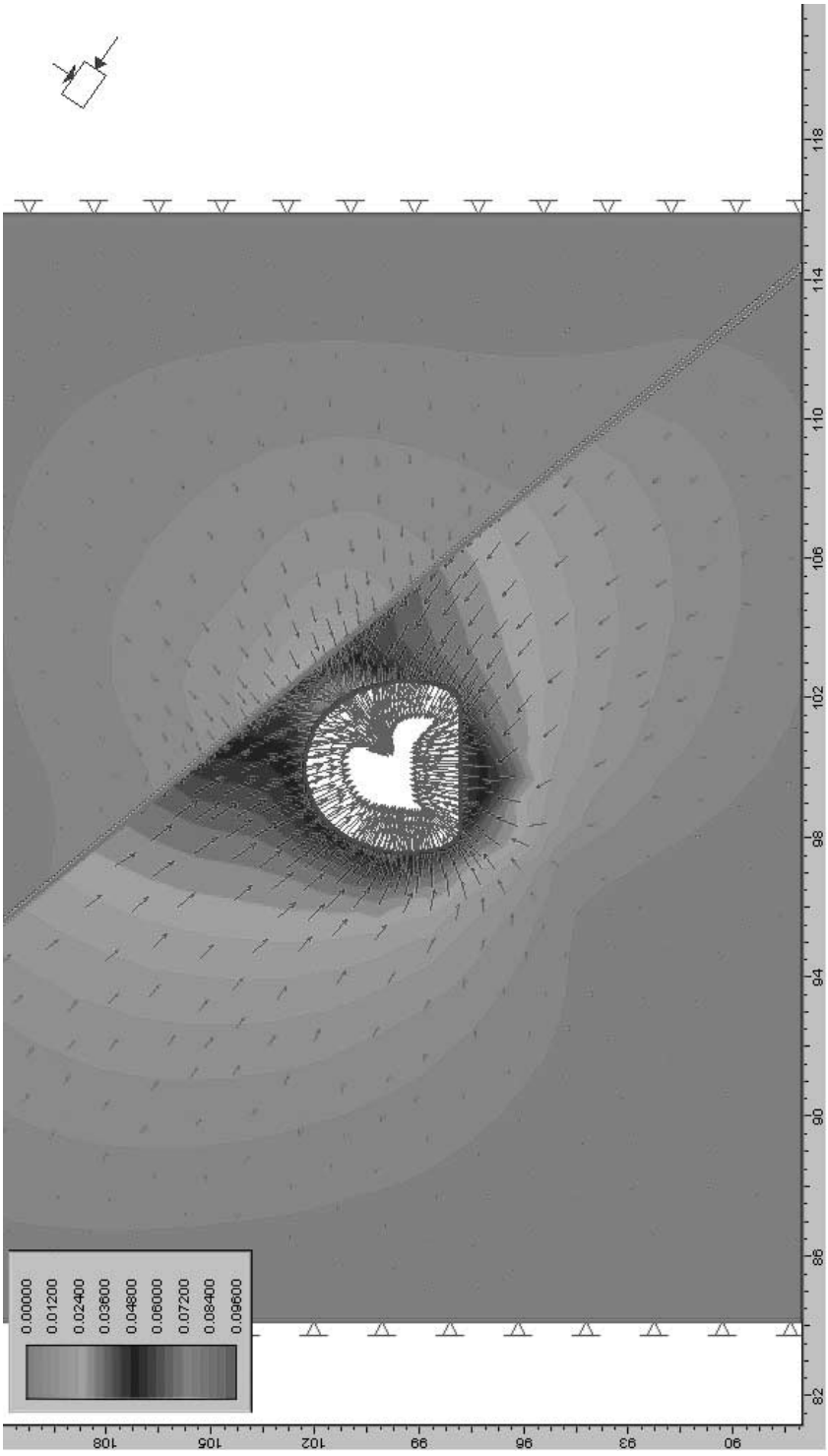


*Figure 10.* (a) Example 4. Displacement vectors, and contours of displacement magnitudes (m) when the 'real' boundary state of stress is applied. Difference between stage 2 (end of geodetic measurements) and stage 1 (beginning of geodetic measurements).

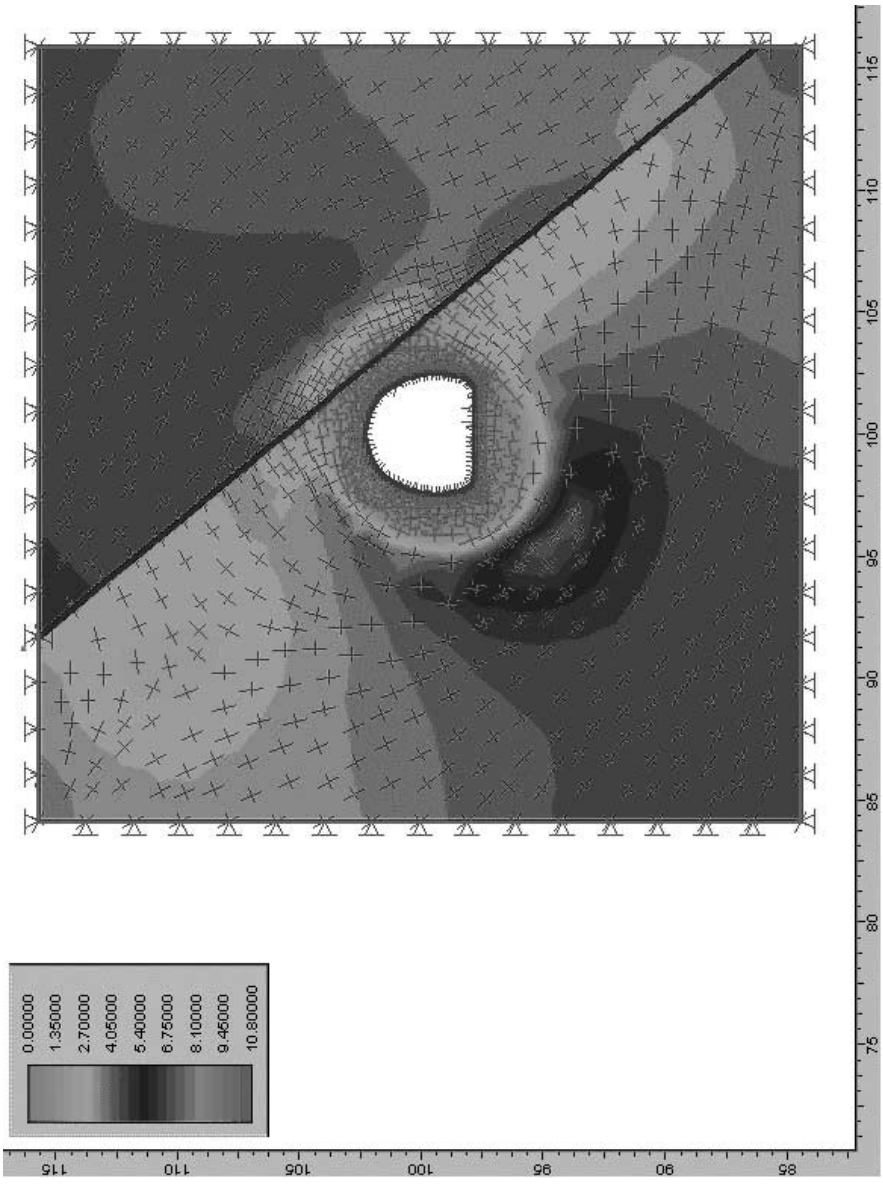


*Figure 10.* (b) Example 4. Contours of maximum principal stresses (MPa), and principal stress directions when the 'real' boundary state of stress is applied. Difference between stage 2 (end of geodetic measurements) and stage 1 (beginning of geodetic measurements).

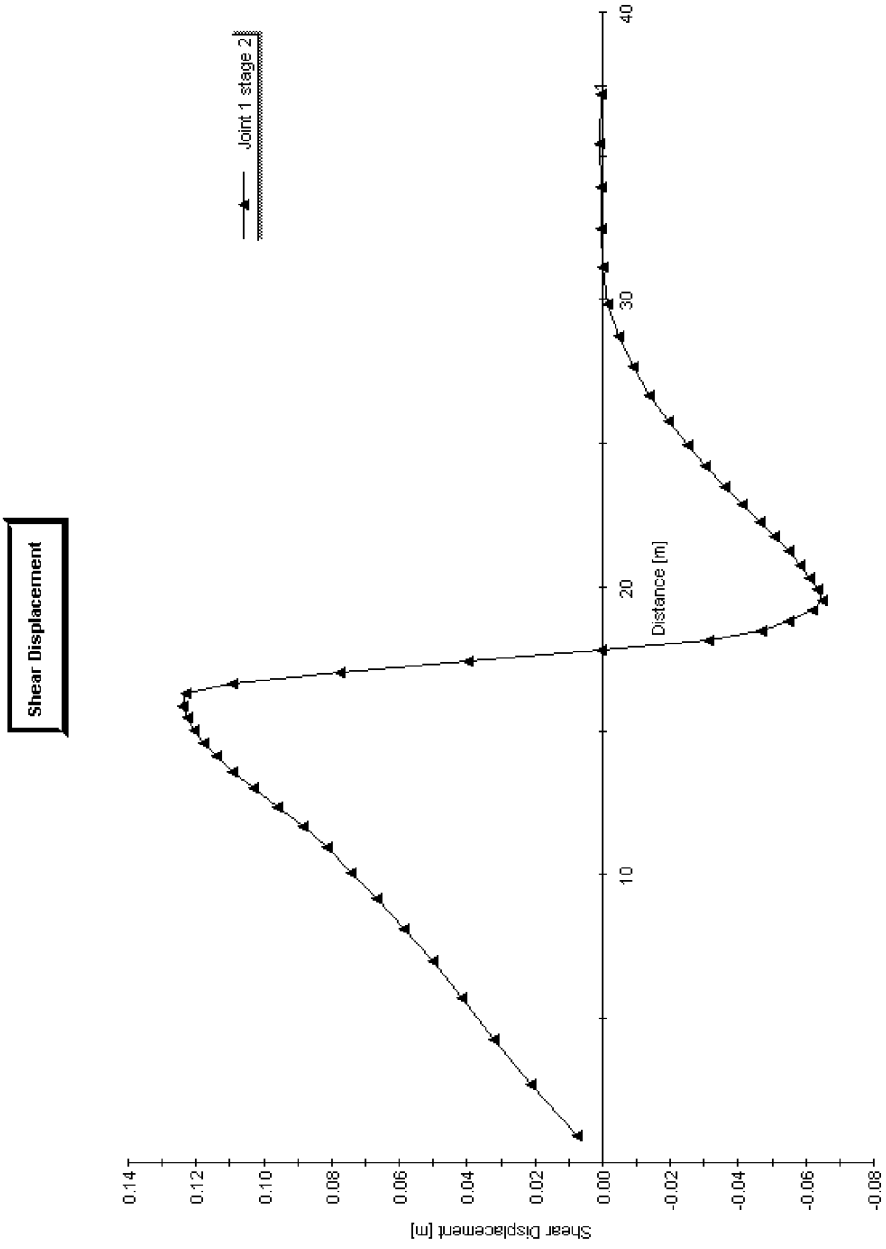


*Figure 10.* (c) Example 4. Shear displacements along the fault (m) induced by the tunnel excavation when the 'real' boundary state of stress is applied. Difference between stage 2 (end of geodetic measurements) and stage 1 (beginning of geodetic measurements).

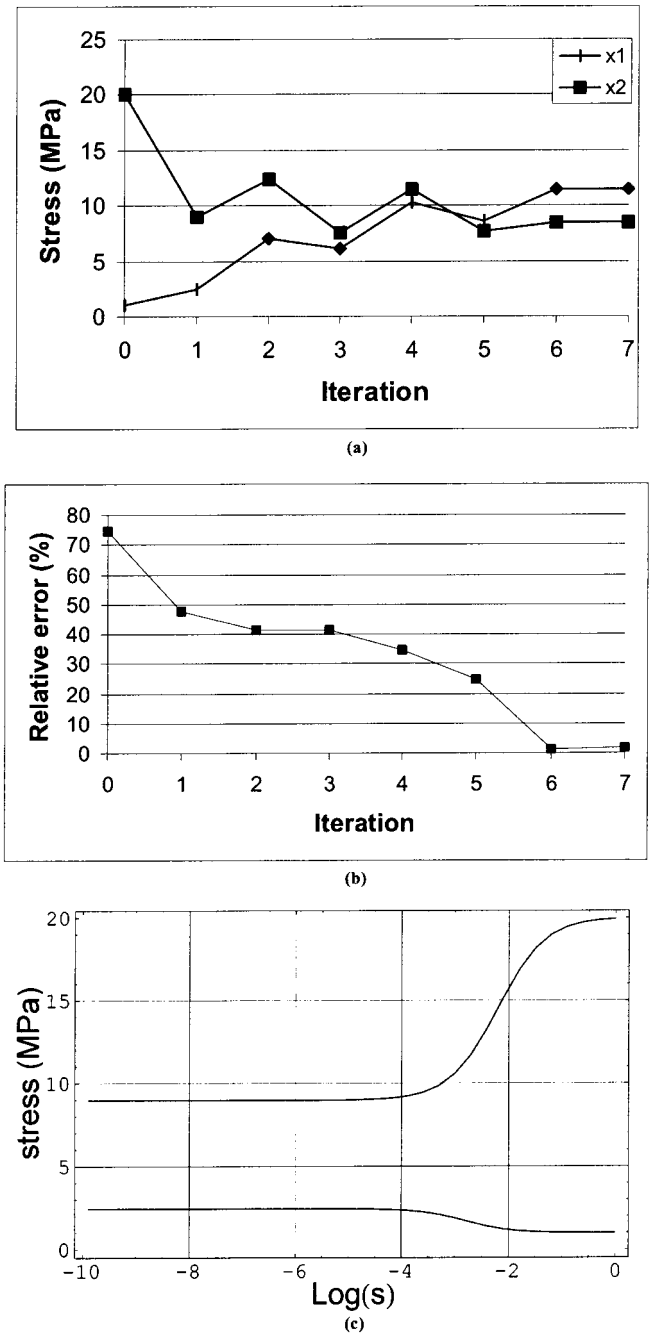


*Figure 11.* Example 4. (a) Computed boundary stresses at each iteration (iteration = 0 refers to the starting state of stress); (b) square mean root of the difference calculated-measured displacements at each iteration; (c) best estimates of boundary stresses versus $S$ at the first iteration using absolute displacements as observed data.

Table 11. *Example 4. Estimated stresses and relative error.*

| Iteration $j$ | $(x_1^j, x_2^j)$ (MPa) | $R_j = \sqrt{\frac{\sum_k^8 \left(\xi_k^{j+1} - y_k\right)^2}{\sum_k^8 (y_k)^2}}$ (%) |
|---|---|---|
| 0 | (1,20) | 74.4 |
| 1 | (2.4474, 8.9735) | 47.6 |
| 2 | (7.0821, 12.3695) | 41.4 |
| 3 | (6.1151, 7.5130) | 41.3 |
| 4 | (10.2772, 11.5197) | 34.6 |
| 5 | (8.5978, 7.6772) | 24.8 |
| 6 | (11.3935, 8.5011) | 1.5 |
| 7 | (11.4720, 8.5210) | 1.8 |

## Acknowledgements

This research is funded by National Science Foundation under grant no. CMS-9713559. The authors would like to thank Professor Frangopol (University of Colorado at Boulder, CO, USA) for valuable discussion on the uncertainty aspects of this paper, and Professor Schubert (Technical University, Graz, Austria) for providing them with the results of his research on modern geodetic monitoring programs for tunnels

## References

Barla, G. and Gioda, G. (1983). *Un esempio di interpretazione delle misure di convergenza in galleria*, In *Proc. XV Convegno nazionale di Geotecnica.* Spoleto, Italy. pp. 281–286.

Curran, J. H. and Corkun, B. T. (1998) Phase2. 2D finite element program for calculating stresses and estimating support around underground excavations. *Reference Manual and Tutorial Manual.* Rockscience, Toronto, Canada.

Gioda, G. and Maier, G. (1980) Direct search solution of an inverse problem in elastoplasticity: identification of cohesion, friction angle and *in situ* stress by pressure tunnel tests, *Int. J. Num. Meth. Engng*. **15**, 1823–1848.

Hoek, E. and Brown, E. T. (1980) *Underground Excavations in Rock*, Institution of Mining and Metallurgy, London.

Lewis, T. O. and Odell, P. L. (1971) *Estimation of Linear Models*, Prentice-Hall, Englewood Cliffs.

Mase, G. E. (1970) *Continuum Mechanics*, McGraw-Hill, New York.

Mardsen, J. E. and Hughes, T. J. R. (1994) *Mathematical Foundations of Elasticity*, Dover, New York.

Menke, W. (1989) *Geophysical Data Analysis: Discrete Inverse Theory*, Academic Press, San Diego.

Purrer, W. (1997) Geotechnical based procedures in tunneling, *Felsbau*. **15**(3), 222–224.

Rabensteiner, K. (1996), Advanced tunnel surveying and monitoring, *Felsbau*. **14**(2), 98–102.

Sakurai, S. (1997) Lessons learned from field measurements in tunnelling, *Tunnelling and Underground Space Technology*. **12**(4), 453–460.

Sakurai S. and Akutagawa, S. (1995) *Some aspects of back analysis in geotechnical engineering,* In *Proc. EUROCK '93*. Libsbon, Portugal, Balkema, Rotterdam. pp. 1133–1140.

Sakurai, S., Akutagawa, S. and Kawashima, I. (1993) *Back analysis of non-elastic behaviour of soils and heavily jointed rocks*. In: *Proc. 2nd Asian-Pacific Conference on Computational Mechanics*, Sidney, Australia. Balkema, Rotterdam. pp. 465–469.

Schubert, W. and Steindorfer, A. (1996) Selective displacements monitoring during tunnel excavation, *Felsbau*. **14**(2), 93–97.

Tonon, F. (2000) *Three-dimensional Modeling of Underground Excavations and Estimation of Boundary Conditions in Rock with Fabric*, Ph.D. dissertation, University of Colorado at Boulder.

Tonon, F., Amadei, B. and Frangopol, D. M. (2000) *Estimation of boundary conditions in tunneling using a Bayesian approach*, In: *Proc. 8th ASCE Joint Specialty Conf. on Probabilistic Mechanics and Structural Reliability*. ASCE, Reston. Paper 253.

Tonon, F. Amadei, B. and Pan, E. (submitted) Bayesian estimation of boundary conditions for rock mass models – I. Theory, *Int. J. Rock Mech. Min Sci.*

Wiles, T. D. and Kaiser, P. K. (1994a) In situ stress determination using the under-excavation technique – I. Theory, *Int. J. Rock Mech. Min. Sci. & Geomech. Abstr*. **31**(5), 439–446.

Wiles, T. D. and Kaiser P. K. (1994b) In situ stress determination using the under-excavation technique – II. Applications, *Int. J. Rock Mech. Min. Sci. & Geomech. Abstr*. **31**(5), 447–456.

Yang, L. and Sterling, R. L. (1989) Back analysis of rock tunnel using Boundary Element Method, *J. Geotech. Div. ASCE*. **115**(8), 1163–1169.